Benchmark testing of numerical approaches for modelling the influence of undercut depth on caving, fracture initiation and subsidence angles associated with block cave mining

K.-S. Woo[1,2]*, E. Eberhardt[2], D. Elmo[3], D. Stead[4] and P. K. Kaiser[5]

This paper reports the findings from a benchmark study testing several numerical methods, with a focus on the influence of undercut depth on block caving-induced surface deformation. A comparison is drawn between continuum *v.* discontinuum treatments of the modelled geology. Results were evaluated with respect to different simulated levels of ground disturbance, from complete collapse to small-strain subsidence. The results show that for a given extraction volume, the extent of ground collapse at surface decreases as undercut depth increases. The presence of sub-vertical faults was seen to limit the extent of the modelled caving zones. In contrast, the extent of small-strain surface subsidence was seen to increase with increasing undercut depth. The faults in this case did not have the same limiting effect. Overall, the findings emphasise the importance of balancing model simplification against the need to incorporate more complex and computationally demanding representations of the rock mass structure.

Keywords: Block caving, Caving-induced subsidence, Numerical modelling, Continuum, Discontinuum, Brittle fracture, 2-D *v.* 3-D

This paper is part of a special issue on Block Caving

Introduction

Complexity in geology and brittle tectonics (jointing, faulting, etc.) make rock masses a challenging material to represent mathematically in numerical models. First, numerical methods vary widely in their mathematical formulations, such that a capability favourable for one type of engineering application may be a disadvantage for another. Second, a balance must be struck between the appropriate level of detail and the computing time that will be required to perform a large number of simulations; the scale of the problem being modelled may be substantially larger than the geological features that can be explicitly resolved by the model. Consequently, some numerical methods (e.g. finite element, finite difference) provide computational efficiencies, especially in 3-D, by treating the problem domain as a continuum. Other methods allow the rock mass to be treated as a discontinuum (e.g. distinct element, discrete element) where the presence of geological structures are explicitly modelled together with their influence on the rock mass response and failure kinematics. However, this added complexity comes at the expense of more computationally demanding models.

Both approaches have been applied to the modelling of block caving and caving-induced subsidence. Continuum methods have been favoured as a means to accommodate large 2-D and 3-D block caving models and to perform sensitivity analyses where a large number of model runs are required (Sainsbury, 2012). In other studies, discontinuum methods have been favoured in recognition of the important role discontinuities play with respect to *in situ* fragmentation and failure kinematics during caving (Albrecht *et al.*, 2010). An additional consideration is the importance of brittle fracturing between non-persistent joints in the caving process (i.e., primary fragmentation). This imposes additional computational challenges as it requires a hybrid approach that integrates continuum-based fracture mechanics and discontinuum-based contact detection and interaction principles, such as those available in the finite-/discrete-element (FDEM) approach (Munjiza, 2004; Owen *et al.*, 2004). Advantages include a better description of the physical processes involved and a more realistic representation of the heterogeneities and anisotropy encountered in natural jointing (Vyazmensky *et al.*, 2010; Elmo and Stead, 2010); however, this is attained at the expense of increased computational effort.

Detailed summaries of these numerical methods and their application to different geotechnical problems are discussed in Stead *et al.* (2006) and Hudson and Feng (2010). In this study, benchmark testing of several different numerical techniques was carried out to investigate their

[1]AMC Consultants (Canada) Ltd, Vancouver, Canada
[2]Geological Engineering – EOAS, University of British Columbia, Vancouver, Canada
[3]Mining Engineering, University of British Columbia, Vancouver, Canada
[4]Resource Geotechnics, Simon Fraser University, Burnaby, Canada
[5]RTC-UMC, Centre for Excellence in Mining Innovation, Sudbury, Canada

*Corresponding author, email kyuseokwoo@gmail.com; kwoo@amcconsultants.com

Published by Maney on behalf of the Institute and The AusIMM
Received 26 August 2013; accepted 22 April 2014
DOI 10.1179/1743286314Y.0000000063

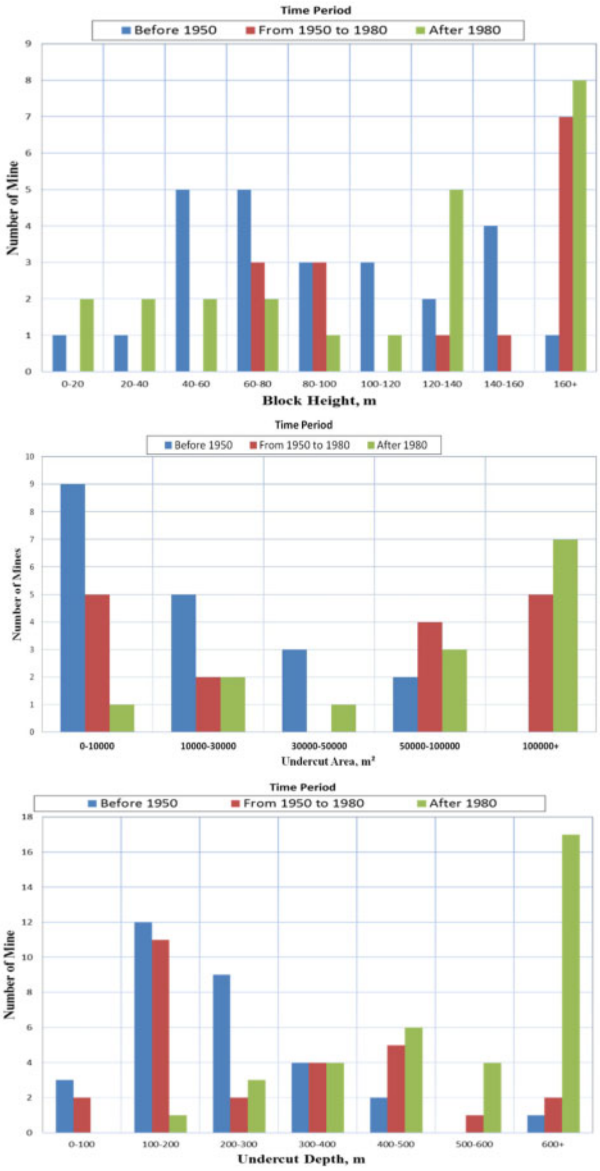

1 Breakdown of block heights, undercut areas and undercut depths associated with historic and current block/panel caving operations. After Woo *et al.* (2013)

capabilities and limitations with respect to modelling block caving subsidence for a range of undercut depths with added consideration of the influence of structural geology. The comparison carried out here focuses on a conceptual problem geometry involving a porphyry copper type deposit, incorporating boundary faults (relative to the ore body and block being caved), several different lithologies and varying rock mass properties. The undercut depths modelled vary from 500 to 2000 m below surface in increments of 500 m using the 2-D continuum code Phase2, the 3-D continuum code FLAC3D, the 2-D discontinuum code Universal Distinct Element Code (UDEC) and the 2-D hybrid FDEM brittle fracture code ELFEN. The modelling scenario selected was based on recent trend towards larger block heights (>200 m), larger undercut footprints (>100 000 m^2) and deeper undercuts (>600 m), compared to historical data (Fig. 1; Woo *et al.*, 2013). For example, with respect to deep undercuts, the Resolution project in Arizona, USA, is proposing mining depths approaching 2000 m, a depth that will certainly challenge the industry's collective experience.

Benchmark study

Model scenario and numerical modelling codes used

Four different numerical modelling codes commonly used in geotechnical practice were compared as part of this benchmark study: Phase2, FLAC3D, UDEC and ELFEN (Rocscience, 2009; Itasca Consulting Group, 2009, 2010; Rockfield, 2009, respectively). Each was applied to the same conceptual scenario specified by the Centre for Excellence in Mining Innovation's Rio Tinto Centre for Underground Mine Construction (RTC-UMC) as part of a larger study on modelling approaches (Bullock *et al.*, 2012). The scenario involves a deep block caving operation in a geologically complex 3-D setting, involving a porphyry-type deposit to be mined in three 500 m wide panels (A towards C in Fig. 2). The ore body and surrounding host rock incorporate several faulted lithologies, with the faults located beside the ends of the undercut. For 2-D modelling, section A–B in Fig. 2 was used.

Figure 3 shows the corresponding model geometry used for the 2-D continuum simulations using Phase2. Phase2 is a 2-D finite-element code with the ability to include small-strain joint elements. The external limits of the model were determined based on preliminary elastic modelling, which suggested a 2-D model 10 500 m in length and 4200 m in depth would be sufficient to cover the full lateral extent of measurable surface subsidence. Phase2 models with and without joint elements were compared to determine the influence of small-strain joint movements on the modelled surface subsidence. The joint elements were introduced to the continuum mesh using a discrete fracture network (DFN) model comprised of two orthogonal joint sets of variable spacing and persistence dipping at 0 and 90° (Fig. 3). This orientation was selected to minimise the degree of asymmetry due to the joint sets and allow a more direct comparison between the different modelling methods. Mine data (Woo *et al.*, 2013) and numerical modelling (Vyazmensky *et al.*, 2010), both show that caving-induced subsidence incorporates significant asymmetry in the ground deformation profile due to the presence of dipping geological structures.

The continuum modelling was extended to 3-D using the finite-difference code FLAC3D (Fig. 4). As a 3-D continuum-based tool, FLAC3D does not easily allow the introduction of faults and joints into the model and requires each discrete feature to be manually specified through matching interfaces thereby entailing significant pre-processing preparation time. In this case, only the large bounding faults were inserted into the FLAC3D model, with the added simplification of modelling these as vertical instead of steeply dipping.

The discontinuum-based modelling was carried out using the 2-D UDEC, which models the problem domain as an assemblage of interacting deformable blocks bounded by joint contacts that are free to open, close or slip in response to excavation or caving. Figure 5 shows the different simple joint patterns used. These include the same 0 and 90° joint pattern used in Phase2 (Fig. 5*b*) and a second pattern superimposed with joints at 45 and 135° (Fig. 5*c*) to increase the degrees of freedom for joint slip and vertical subsidence. A joint spacing of 10 m was used in the area of interest above the undercut and simulated cave (Fig. 5*a*).

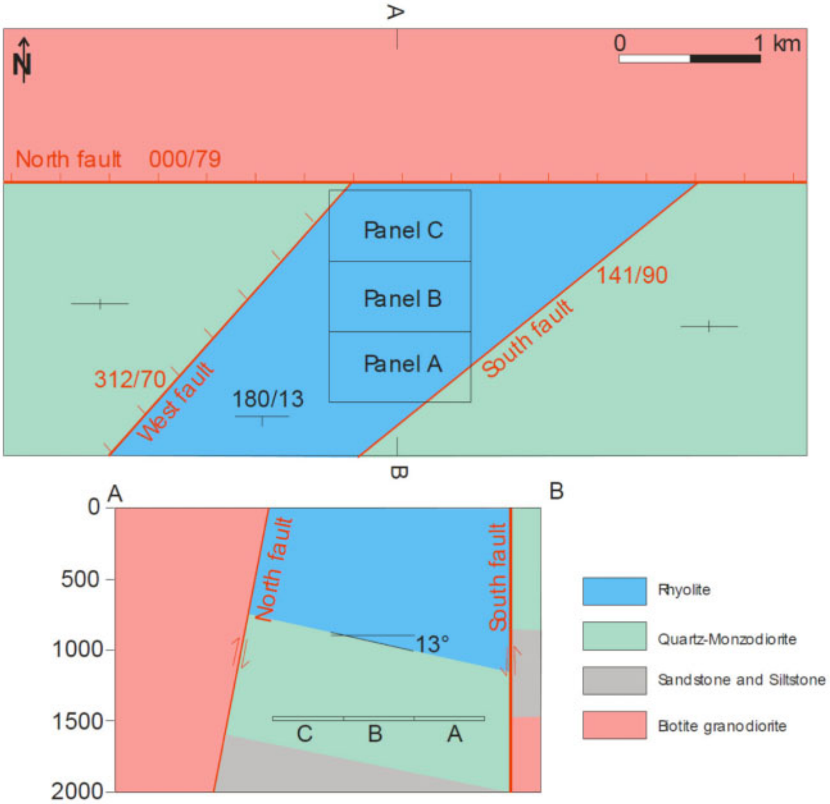

2 Conceptual cave mining geometry used for benchmark study. After Bullock *et al.* (2012)

Lastly, the hybrid modelling was carried out using the FDEM brittle fracture code ELFEN. The same DFN used for the Phase2 model was embedded into the continuum problem domain in the 2-D ELFEN model (Fig. 6). The model was developed to explicitly model cave propagation through brittle fracturing in response to ore extraction.

Rock mass properties and *in situ* stress

Depth-dependent rock mass properties were used based on the UCS, m_i and GSI values reported in Table 1. These inputs were based on typical values specified by the RTC-UMC (Bullock *et al.*, 2012). Hoek *et al.*'s (2002) empirical relationships based on the Hoek–Brown failure

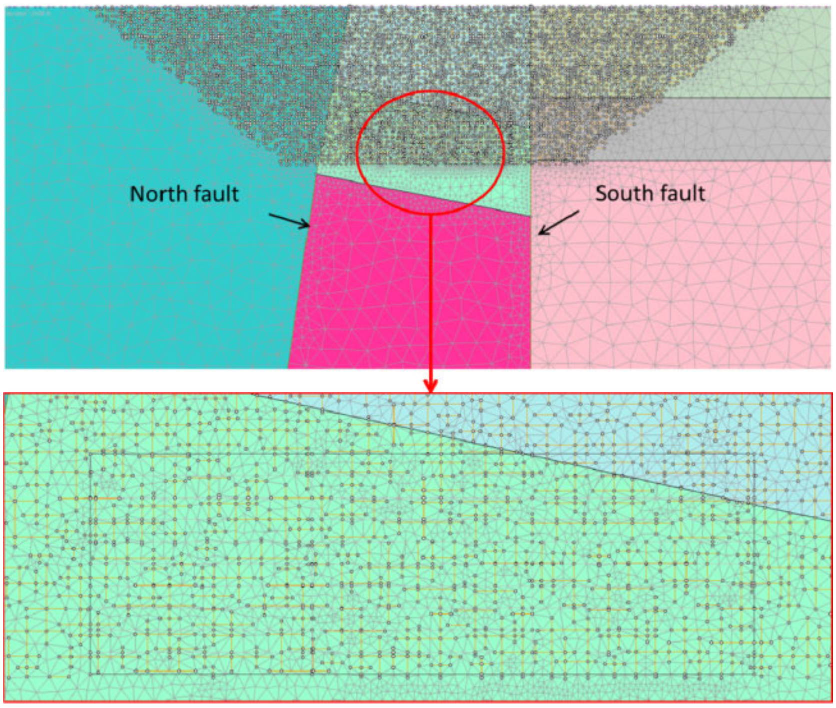

3 Phase2 model geometry for the 2000 m deep undercut simulation, showing the variable orientation, spacing and persistence of joint elements introduced above the undercut. For scale, the model is 10 500 m in length and 4200 m in depth

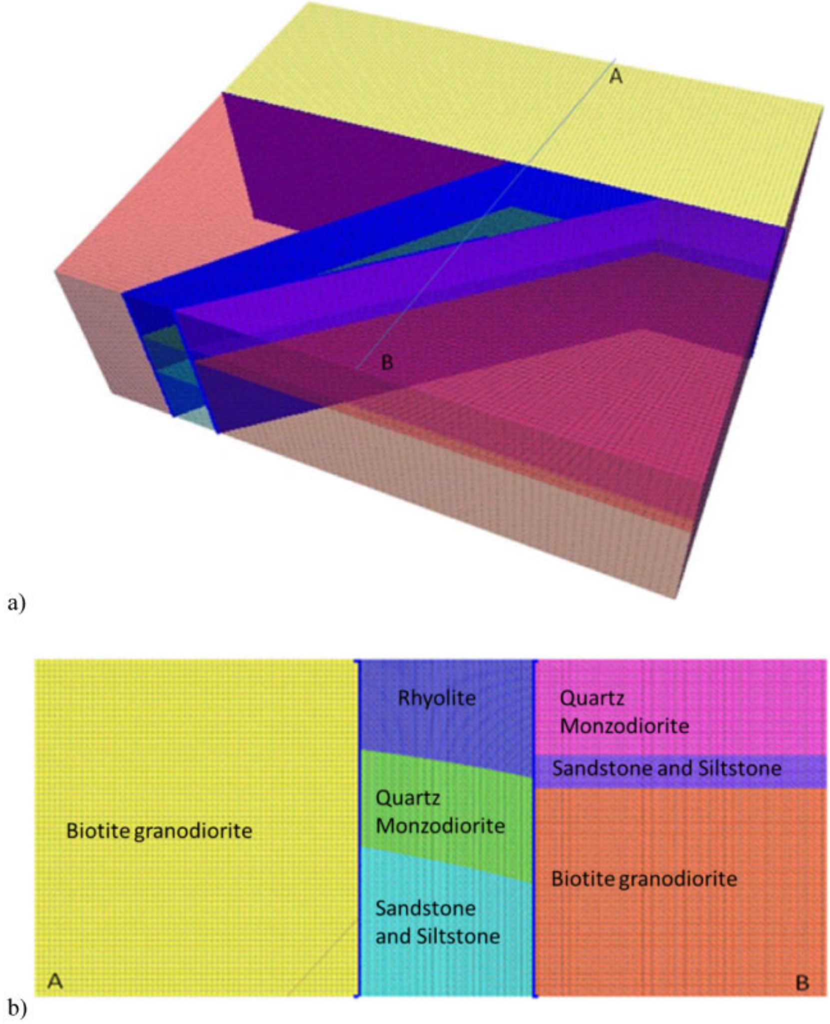

4 FLAC3D model geometry: *a* 3-D perspective, with semi-transparency to show projection of the bounding faults through the model (dark blue) and *b* north and south cross-section showing the fault interfaces in dark blue

criterion were used to derive the rock mass scaled properties. As not all codes have fully implemented a Hoek–Brown constitutive model, the Hoek–Brown values were converted to Mohr–Coulomb by fitting an average linear Mohr–Coulomb relationship to the non-linear Hoek–Brown envelope over the appropriate range of confining stresses (Table 2). Tensile strength (T_{rm}) was estimated assuming a 25% tensile cutoff applied to the theoretical Mohr–Coulomb value. The rock mass deformation modulus, E_{rm}, was calculated using Hoek and Diederichs' (2006) empirical relationship. A fracture energy release (G_f) value of 43 J m^{-2} was applied for brittle fracturing in the ELFEN modelling.

Contact properties for the joint elements and discrete elements were assigned assuming a linear Mohr–Coulomb slip criterion. The north and south faults, the DFN joints and in the case of ELFEN any new fractures generated during the simulation of caving, were given the same values: a joint cohesion of zero and a joint friction angle of 30°. The mechanical contact forces that govern the interactions between discrete elements in UDEC and ELFEN can be loosely defined as the forces that are required to prevent blocks from interpenetrating. A normal stiffness of 4 GPa m^{-1} and shear stiffness of 0·4 GPa m^{-1} were assumed. The values reported in Table 2 were applied uniformly to the Phase2, UDEC and ELFEN models. The rock mass properties were reduced by 75% for the FLAC3D models to account for the larger mesh size.

The initial stress conditions were implemented as specified for the Centre for Excellence in Mining Innovation (CEMI) RTC-UMC benchmarking exercise (Fig. 7; Bullock *et al.*, 2012). The vertical stress is defined as gravitational loading with a rock unit weight of 27 kN m^{-3}. The maximum horizontal stress (σ_{Hmax}) is assumed to be 1·9 times the vertical stress and is aligned north–south. The minimum horizontal stress (σ_{Hmin}), aligned east–west, is assumed to be 1·2 times the vertical stress.

Simulation of draw and caving

The simulation of cave propagation is a key consideration given its direct relationship to the caving-induced deformations being modelled. For the continuum methods, caving was implemented through an implicit approach where the geometry of the cave is built into the model (as opposed to explicitly modelling the caving process). This is a key limitation of applying continuum techniques to block caving problems. The implicit approach employed in the Phase2 and FLAC3D assumes a cave geometry at several different points in time in overall cave development and an incremental

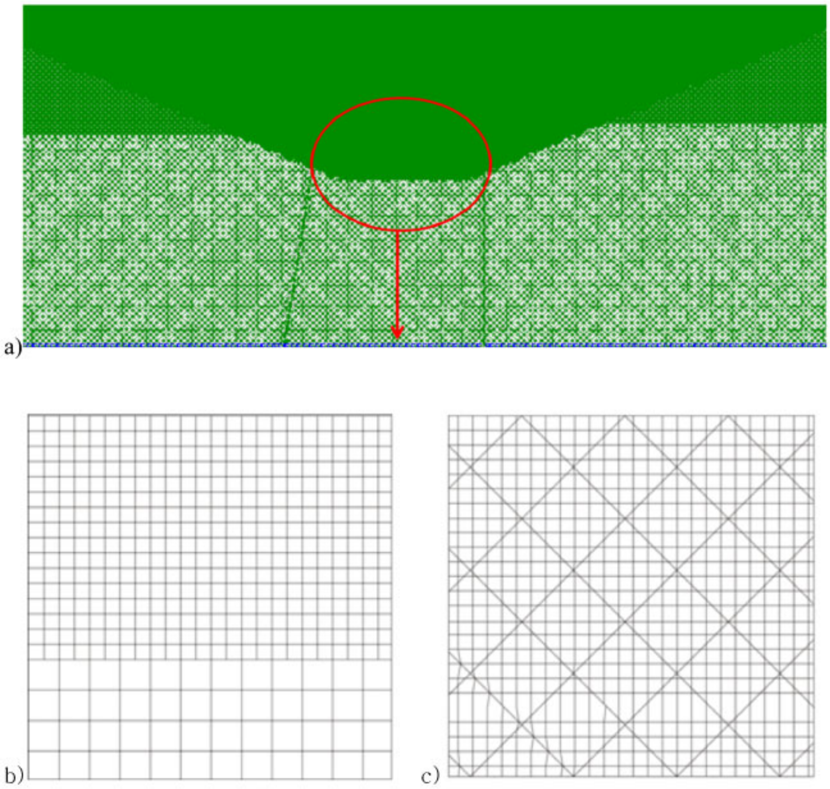

5 *a* Universal distinct-element code (UDEC) model geometry for the 2000 m deep undercut simulation, showing close-up of: *b* orthogonal joint pattern at 0 and 90° and *c* second joint pattern superimposed at 45 and 135°. Note for scale that the lower close-up views are 250 by 250 m

change in the corresponding element properties from those of intact ore to fragmented rock. A simplified cave geometry was assumed involving caving in 50 m increments up to a total block height of 200 m. Caving is initiated in Panel A and progresses through two stages (100 m cave height) before the next panel, Panel B, is initiated (Fig. 8). This is continued for each panel until the cumulative height of caved rock area reaches 200 m.

Table 2 includes the material properties assumed for the caved rock. To avoid numerical errors resulting from severe mesh distortion, the caved rock material was modelled as an elastic material, using reduced elastic

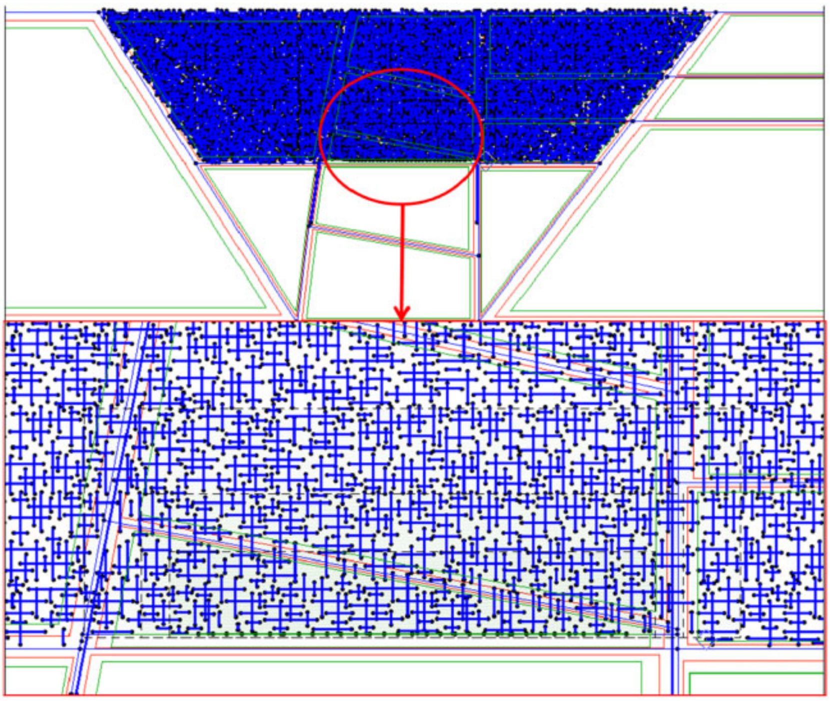

6 ELFEN model geometry for the 2000 m deep undercut simulation, showing close-up of the embedded discrete fracture network used. Note that this is the same discrete fracture network (DFN) as used for the Phase2 models

Table 1 Rock mass properties provided for benchmark study (after Bullock *et al.*, 2012)

	Intact rock			Rock mass			
Lithology	UCS/MPa	Hoek–Brown constant/m_i	Young's modulus/GPa	RMR89	GSI	Block length/m	Joint conditions Jc
Rhyolite	205	25	60	49	44	0·35	0·7
Quartz-monzodiorite	140	20	50	43	38	0·35	0·5
Sandstone and siltstone	125	18	40	52	47	0·5	0·7
Biotite granodiorite	145	22	55	43	38	0·35	0·5

properties to account for the reduced deformation modulus that would be expected for caved rock, as well as allowances for the presence of a small air gap. This procedure requires redefinition of the initial stresses within the caved material to those corresponding to the self-weight of the caved material and not the locked in tectonic stresses initially prescribed for the ore and host rocks.

Simulation of the propagating cave in UDEC was carried out using the same implicit method and mining sequence. The key difference in this case was that the discontinuum treatment of the problem domain provided the added freedom for blocks to move along the joint interfaces (i.e. shear), enabling large displacements to develop in the model.

In ELFEN, modelling of the draw and caving process was carried out explicitly following procedures developed by Elmo *et al.* (2010). The caving algorithm removes all meshed elements whose centroids are located within a specified region, in this case corresponding to the undercut/production level. An iterative process is used such that the removal of elements is repeated continuously at a given numerical time step in order to return the specified draw rate (Fig. 9). No hang ups at the extraction level were simulated; an ideal draw scenario was assumed in the model.

Numerical analysis results

The results for each modelling method were plotted assuming a lower-bound vertical displacement cutoff of 1 m (Figs. 10–15). Comparison of the Phase2 models without and with joints (Figs. 10 and 11, respectively), show that the extent of the subsidence profile increases with the presence of the orthogonal joints by 3 and 8% for the 1500 and 2000 m deep undercuts, respectively. This is attributed to the weaker (more deformable) rock mass conditions associated with the inclusion of joints. The FLAC3D continuum results (Fig. 12) show a lesser degree of subsidence than the Phase2 continuum analysis, both without joints, due to the 3-D model's ability to redistribute stresses and displacements in the third dimension, thus reducing their magnitude. As the FLAC3D undercut depth increases, the subsidence profile widens and the influence of the bounding faults diminishes. This agrees with the 2-D Phase2 results. It is also noteworthy that the shape of the subsidence profile in 3-D elongates in the north–south direction as the undercut depth increases. This coincides with the longer axis of the panels being modelled (Fig. 2), with the effect becoming more pronounced as the undercut depth increases.

Figures 13 and 14 compare the UDEC discontinuum results. These indicate that the area of subsidence is significantly narrower with the orthogonal joints at 0 and 90° compared to the model with the added set at 45 and 135°. As expected, the presence of the inclined joints promotes more ground movement (slip) in the lateral direction. Figure 14 shows this response increasing with undercut depth. For the 2000 m undercut, the subsidence extends so broadly that it approaches and slightly interacts with the right boundary. The asymmetry observed in these contours is related to the direction of caving, with Panel A to the south being developed first before progressing towards the north with Panels B and C. In all cases (Fig. 14), the results indicate that even with the 45 and 135° joint sets, the zone of caving (vertical displacements greater than 5 m) is limited by the presence of the bounding faults; in contrast, the extent of the smaller-strain subsidence (1 m contour threshold) is seen to increase as a function of undercut depth despite the presence of the bounding faults.

The influence of undercut depth on subsidence using the hybrid FDEM code ELFEN is captured in Fig. 15. Brittle fracturing induced by caving is mostly limited to the area between the bounding faults. In contrast, the pattern of subsidence (1 m contours) is similar to that in the other numerical models, widening with increasing undercut depth without being constrained by the presence of the bounding faults.

Table 2 Depth-dependent Mohr–Coulomb rock mass properties derived for the benchmark study

Lithology	σ_{3max} MPa	Young's modulus E_{rm}/GPa	Cohesion c_{rm}/MPa	Friction angle φ_{rm}/°	Tensile strength T_{rm}/MPa
Rhyolite	7·5–17·5	12·6	3·3–5·9	46–52	0·6–1·2
Quartz-monzodiorite					
Below the undercut	30	7·0	6·5	34	1·8
South of south fault	5–20	7·0	1·9–4·9	38–49	0·4–1·2
Sandstone and siltstone					
Below the undercut	45–50	10·2	9·1–9·7	31–32	2·5–2·8
South of south fault	30–35	10·2	6·9–7·7	34–35	1·8–2·1
Biotite granodiorite					
North of north fault	10–40	7·7	3·2–8·2	33–44	0·7–2·3
South of south fault	40	7·7	8·2	33	2·3
Caved rock	–	0·26	–	–	–

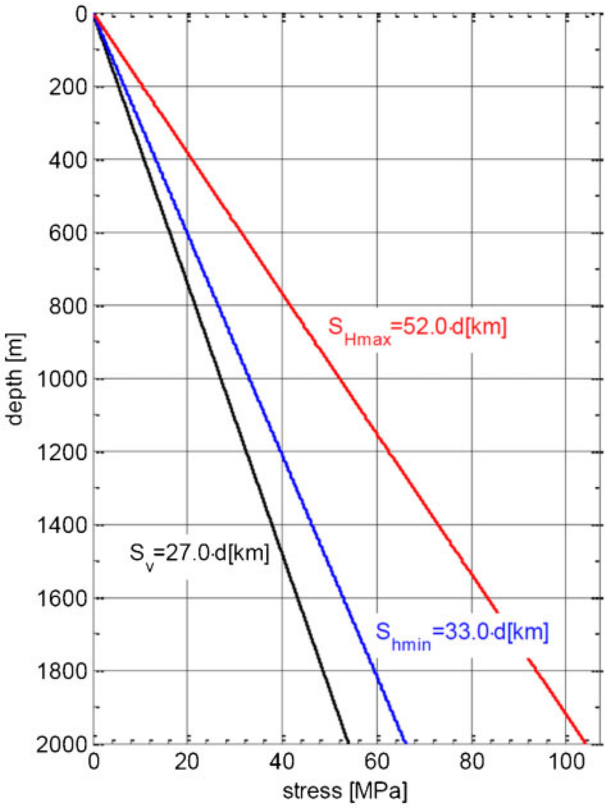

7 ***In situ*** **stress conditions used for benchmark testing: SH_{max} is north–south and Sh_{min} is east–west. After Bullock *et al.* (2012)**

The key consideration in comparing the results for the different undercut depths is that the 'volume' of excavated ore (or block height) in each model is the same. This means a decreasing extraction ratio with increasing undercut depth. In the case of the 500 m deep undercut, 40% of the rock column above the undercut is extracted. For the 2000 m deep undercut, only 10% of the rock column is extracted. Consequently, the modelling results for the 500 m deep undercut clearly show the importance of incorporating a 'realistic' fracture network in the analysis. Comparison of the subsidence profiles clearly indicates that the subsidence zone increases as a function of increasing undercut depth. The zone of caving remains within the bounding faults and its extent actually decreases with increasing undercut depth (i.e. decreasing extraction ratio).

Discussion: caving, fracture initiation and subsidence angles

Woo *et al.* (2013) discuss the importance of macro- and micro-surface deformations related to block caving. Using the definitions of van As *et al.* (2003), these can be quantified as angles measured from the outer boundary of the undercut to the ground surface and the farthest extent of caving (complete ground collapse), fracture initiation (opening of tension cracks and scarps) and subsidence (small-strain ground deformations that can still adversely impact strain-sensitive critical infrastructure). These are depicted in Fig. 16.

A key strength of the hybrid FDEM brittle fracture approach (ELFEN) is that the model output (Fig. 15) allows for direct delineation of the caving, fracture initiation and subsidence angles. For the continuum results (e.g. Phase2), the caving and fracture initiation angles were estimated based on the distribution of yielded elements and vertical displacements (Fig. 17). The fracture initiation angle was correlated to tensile yield indicators. For the discontinuum results (e.g. UDEC), the caving angles were similarly interpreted based on the distribution of shear and tensile yield indicators (Fig. 18). However, the explicit representation of discontinuities in the model allowed the fracture initiation angle to be directly measured based on the extent of joints on surface showing significant opening or slip (Fig. 19). The UDEC results show a pattern of decreasing fracture initiation angles with undercut depth as fracturing/slip extends to the bounding faults, until the undercut reaches 2000 m depth where the reduced extraction ratio results in a diminished extent of fracturing on surface.

Figure 20 compares the caving angles derived from the 2-D continuum (Phase2), 3-D continuum (FLAC3D), discontinuum (UDEC) and hybrid brittle fracture (ELFEN) models. In general, the caving angles indirectly

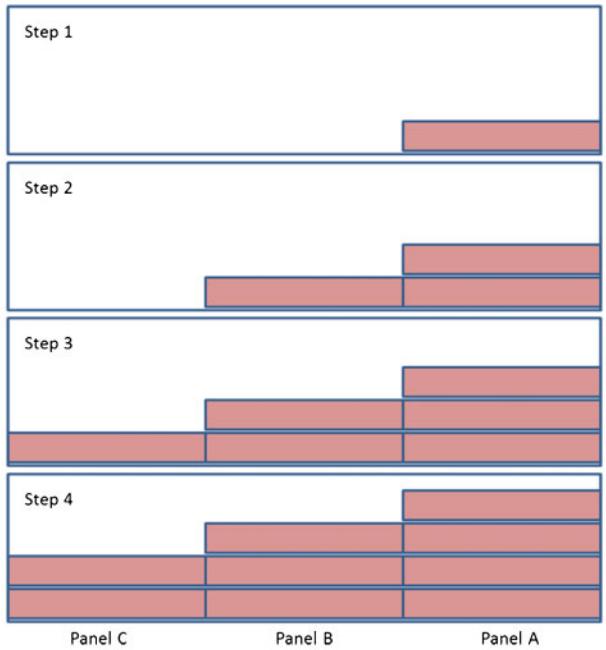

8 Undercut and draw sequence used for Phase2, FLAC3D and universal distinct-element code (UDEC) models

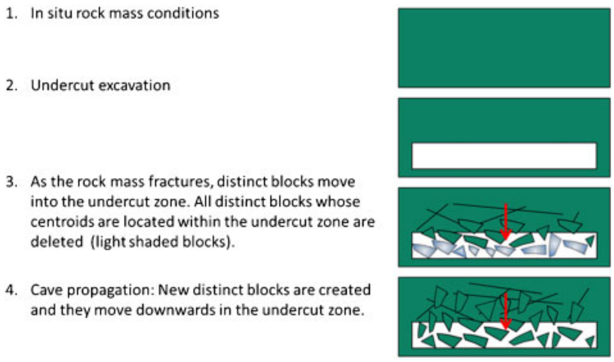

9 Block deletion method used to simulate draw for ELFEN modelling

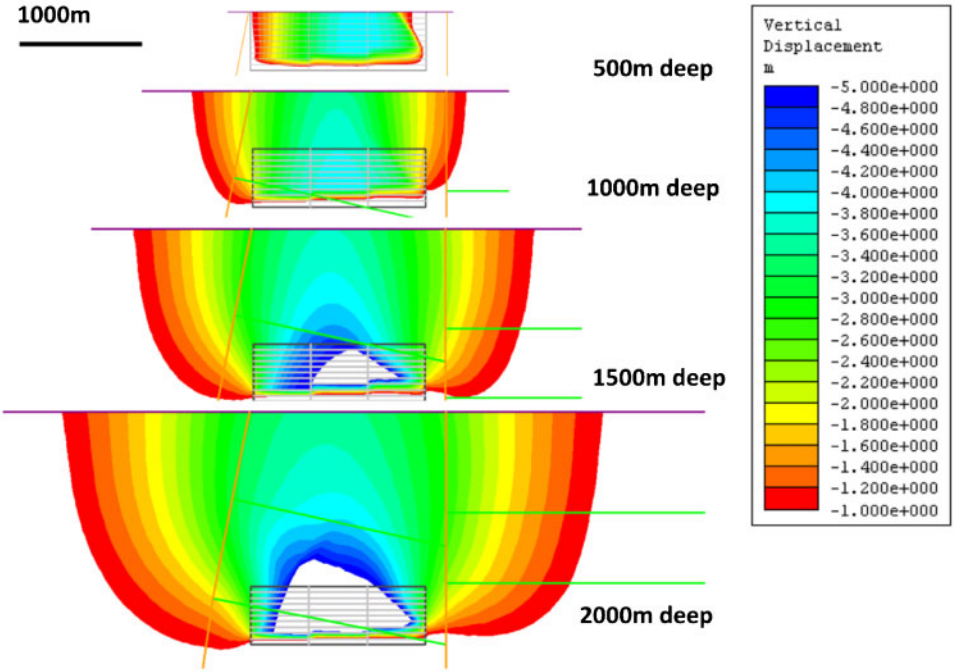

10 Phase2 continuum subsidence results for undercut depths of 500–2000 m. Vertical displacement contours are plotted with a 1 m minimum cutoff

and directly measured indicate near vertical caving angles. The continuum results indicate a slight decrease in caving angle with increasing depth despite the fact the extraction ratio is decreasing. This is considered here to be an artefact and limitation of the method by which the caving angle is interpreted (indirectly using plasticity indicators), together with the interconnected nature of the continuum mesh and the small-strain limitation of the joint elements. The hybrid brittle fracture results more accurately depict increasing caving angles with increasing

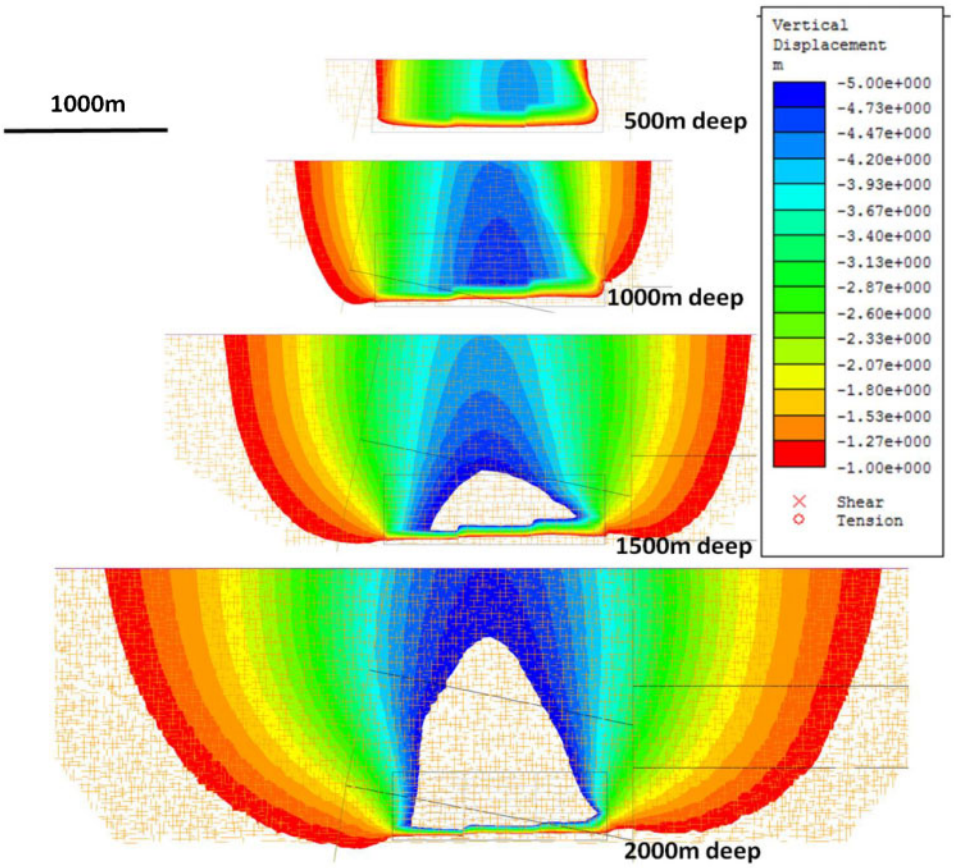

11 Phase2 continuum subsidence results with the inclusion of joint elements, for undercut depths of 500–2000 m (1 m minimum vertical displacement cutoff)

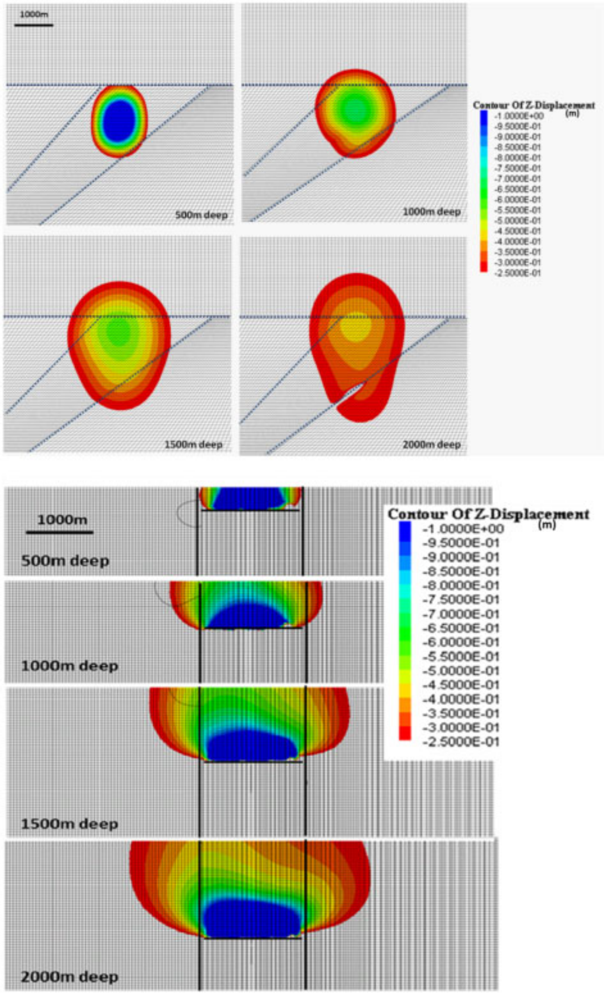

12 FLAC3D continuum subsidence results for undercut depths of 500–2000 m (0·25 m minimum vertical displacement cutoff). Top: surface plan view. Bottom: north–south section

undercut depth, showing overhanging angles (>90°) as the reduction in extraction ratio with depth reduces the extent of caving and ground collapse that migrates to surface. Woo *et al.* (2013) showed similar trends in a comprehensive review of ground deformation data from historic mining operations around the world. Similar trends were seen in the modelling results for the fracture initiation angle (Fig. 21). In general, the fracture initiation angle was seen to be approximately 10–20° lower than the caving angles, with the difference increasing with undercut depth.

The subsidence angles for all models were estimated based on the vertical displacement contours defined by a 1 m lower-bound cutoff (Fig. 22). The angles are seen to generally decrease with increasing undercut depth indicating an increasing extension of the surface subsidence profile. For the UDEC discontinuum results with the 45 and 135° inclined joints, the subsidence angles decrease but then sharply stabilise for the deeper undercuts. The angle of the joint sets is seen to limit the maximum extent of the subsidence zone with the lowest angle coinciding with the dip of the joints (45°). In the ELFEN model, the angle of subsidence decreases with increasing undercut depth indicating that, unlike the caving and fracture initiation angles, the bounding

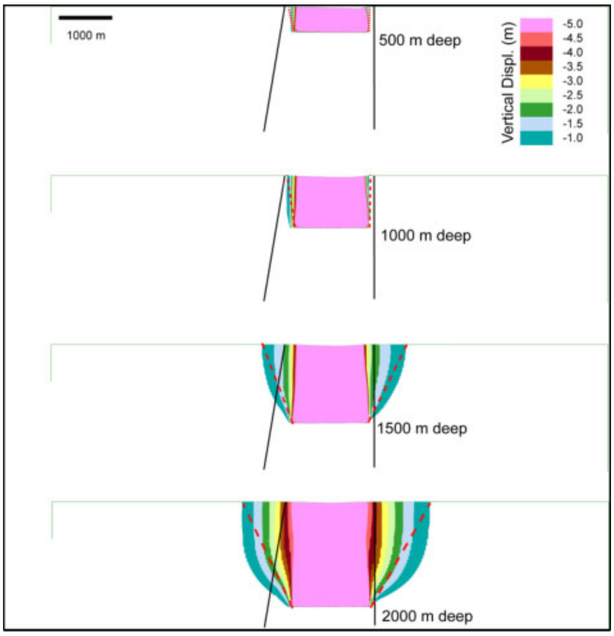

13 Universal distinct-element code (UDEC) discontinuum subsidence results for undercut depths of 500–2000 m with 0 and 90° joint sets (1 m minimum vertical displacement cutoff)

faults do not significantly influence or limit the lateral extent of smaller-strain subsidence. The subsidence angles measured in the ELFEN models further imply a non-linear trend with the extent of subsidence markedly increasing as undercut depths decrease. This perhaps suggests that the bounding faults do have some influence on limiting small-strain subsidence for the shallower undercut depths, but not for the deeper undercuts. A noteworthy observation from the comparison of

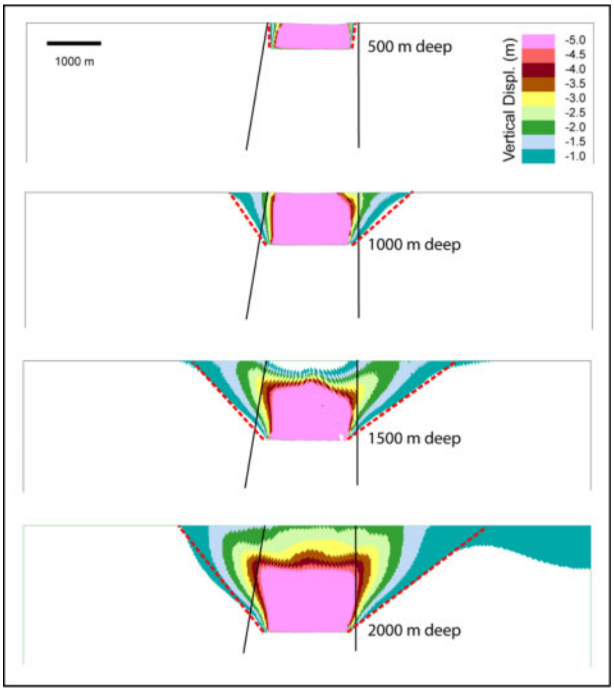

14 Universal distinct-element code (UDEC) discontinuum subsidence results for undercut depths of 500–2000 m with 45 and 135° joint sets (1 m minimum vertical displacement cutoff)

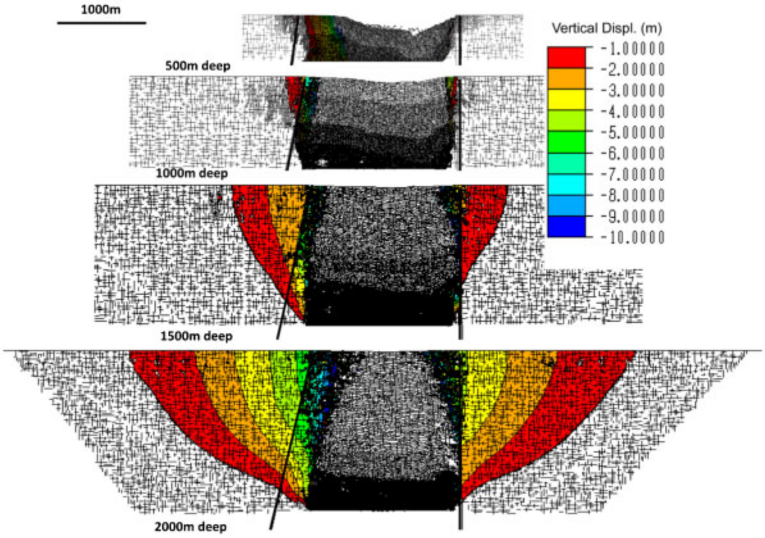

15 ELFEN brittle fracture subsidence results for undercut depths of 500–2000 m (1 m minimum vertical displacement cutoff)

subsidence patterns identified by UDEC (with inclined joint sets) and ELFEN is that although the subsidence angles measured for the undercut depths of 500 and 2000 m do not differ, the differences for the 1000 and 1500 m deep undercuts are considerable. Movement of individual blocks on the inclined joints in response to caving appears to be more active with the shallower undercuts, having a more pronounced influence on the surface subsidence profile.

In the ELFEN results, the influence of the brittle fracture network on the lateral extent of subsidence tends to be less significant for the shallower undercuts, but with greater undercut depths (and higher stresses), brittle fracture activity away from the immediate area above the undercut increases. The trend in subsidence angles with increasing undercut depth for the ELFEN model and the UDEC model with vertical joints is similar. This suggests that the influence of large strain slip along joints in the UDEC models decreases with increasing confining stresses at depth, as would be expected based on a Coulomb slip law.

Conclusions

Results from this benchmark study involving continuum, discontinuum and hybrid brittle fracture numerical modelling methods, showed a similar response with respect to the extent of modelled caving and ground collapse. Caving angles, except in the hybrid FDEM brittle fracture modelling (ELFEN), were seen to decrease with increasing undercut depth resulting in caving angles greater than 90° indicating an overhanging condition with respect to the undercut footprint. Similarly, the extent of macro-deformation in the form of the zone of fracture initiation was also seen to decrease with increasing undercut depth. These responses can be explained as the result of decreasing extraction ratios with increasing undercut depth as the simulation of caving in the models

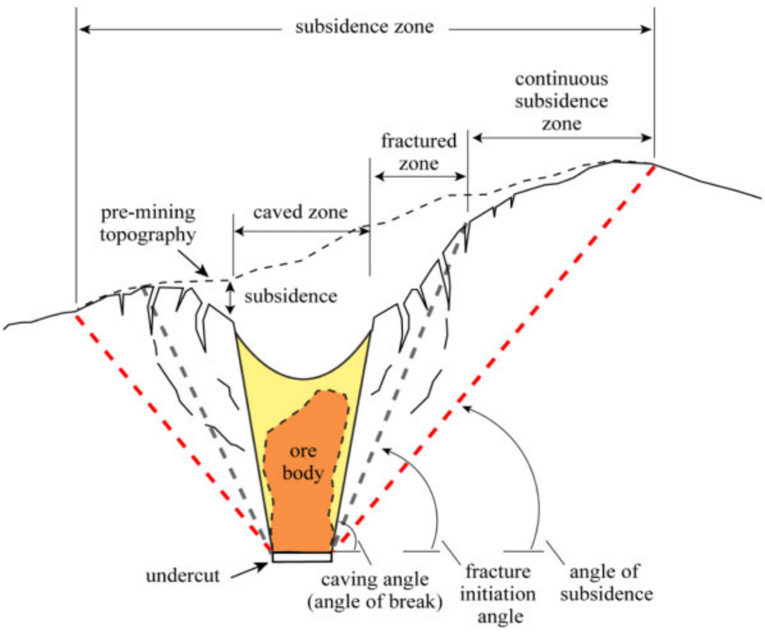

16 Block caving-induced caving, fracture initiation and subsidence deformation zones as defined by van As *et al.* (2003)

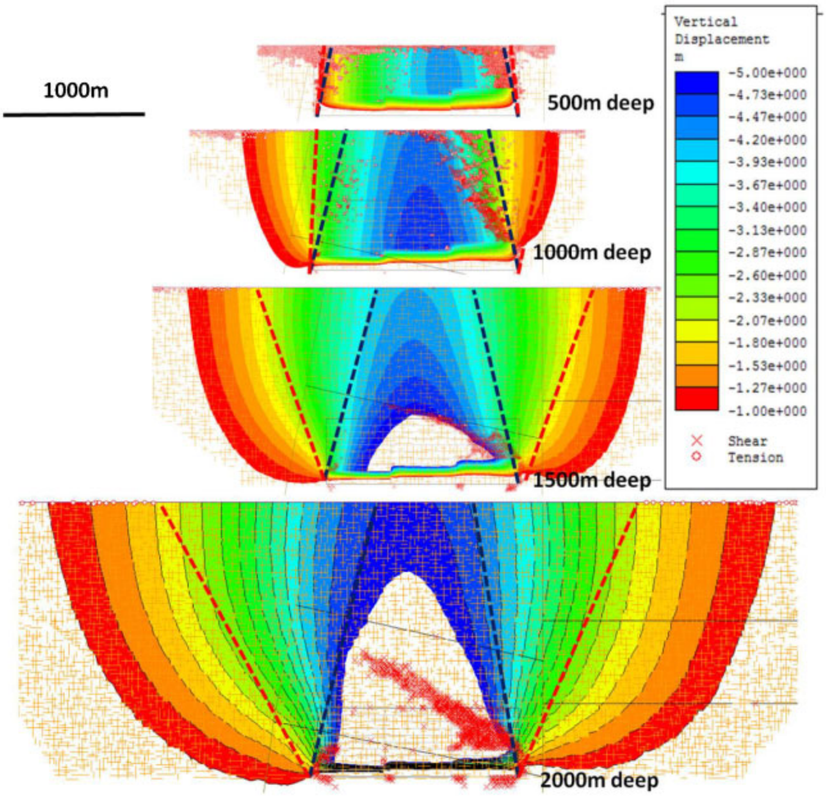

17 Phase2 continuum subsidence results showing delineation of the caving and fracture initiation angles based on yielded elements and vertical displacements. The inside blue dashed lines trace the caving angle, as defined by the zone of shear indicators and vertical displacements >5 m. The outside red dashed lines define the fracture initiation angle based on the zone of tension indicators

maintained the same block height of 200 m. In most cases, the presence of bounding faults on either side of the undercut acted to limit the lateral extent of caving and fracture initiation.

Differences in the results between the different numerical methods emphasise the importance of carefully defining the key objectives of the modelling together with the factors that are most important. Often the need for fast model setup and run times are counter to those for accurate representations of the rock mass fabric (through the inclusion of DFNs) and caving mechanics (brittle fracture). Overall, the 2-D hybrid FDEM approach

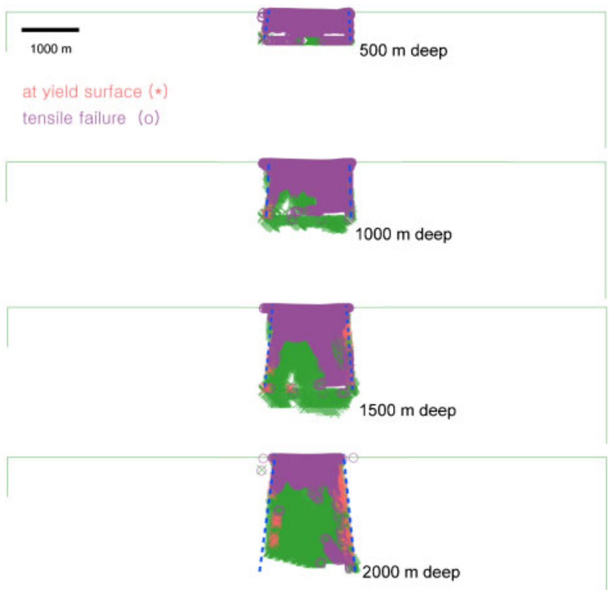

18 Universal distinct-element code (UDEC) discontinuum results showing interpretation of the caving angle (blue dashed line) based on the distribution of shear and tensile plasticity indicators

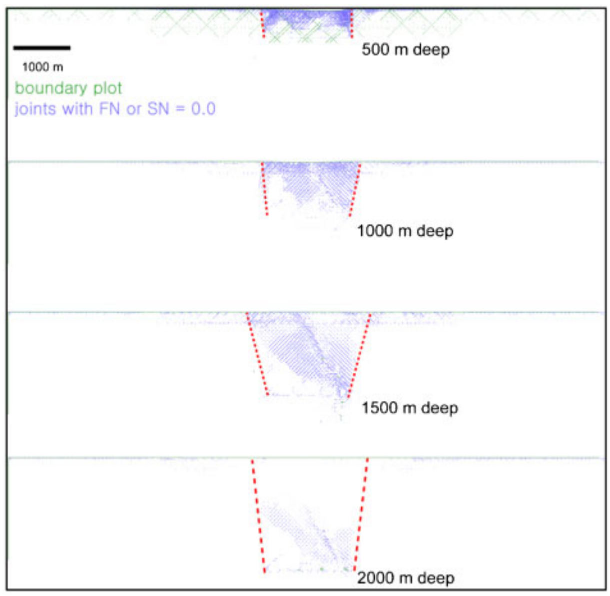

19 Universal distinct-element code (UDEC) discontinuum results showing interpretation of the fracture initiation angle (red dashed line) based on the distribution of shear and tensile plasticity indicators

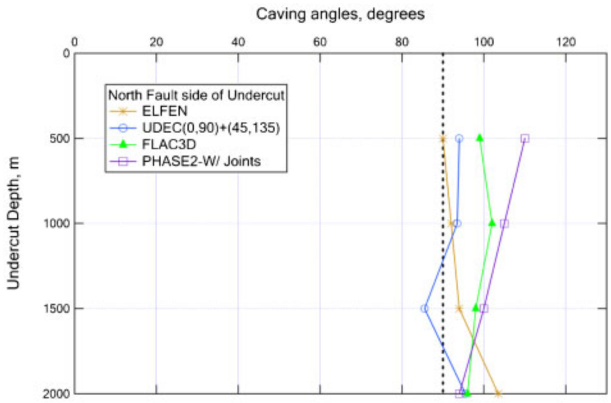

20 **Estimated caving angles *v.* undercut depth, as measured from the north side of the undercut (left hand side in the previous cross-sections)**

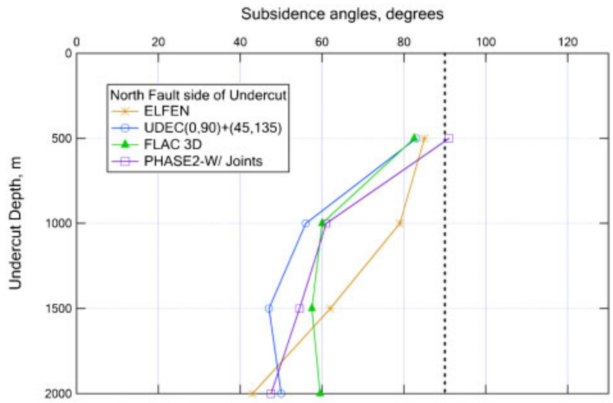

22 **Estimated subsidence angles *v.* undercut depth, as measured from the north side of the undercut (left hand side in the previous cross-sections)**

allowing stress-induced brittle fracturing between joints appeared to provide the more consistent and realistic results. In addition, the contact detection algorithm used allows caving to be more intuitively (explicitly) simulated through a block deletion procedure. Ideally, using a 3-D FDEM brittle fracture code would seem to incorporate all of the key requirements and needs. Computationally, however, this is prohibitively expensive with current computer and software capabilities. Where the need for a 3-D analysis is the over-riding factor, a 3-D finite-element or finite-difference code (e.g. FLAC3D) represents the most viable option at present. This emphasises the importance of establishing a comprehensive understanding of the modelling context from which the numerical code has been developed.

Acknowledgements

This work was supported through funding provided by the Centre for Excellence in Mining Innovation (CEMI) and the Rio Tinto Centre for Underground Mine Construction (RTC-UMC), as well as through a Collaborative Research and Development grant from the Natural Science and Engineering Research Council of Canada (NSERC). The authors would like to thank Keith Bullock and Salina Yong (CEMI) for their technical guidance and assistance in this study.

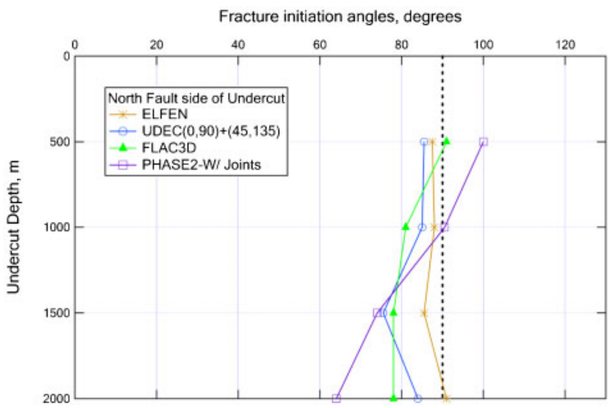

21 **Estimated fracture initiation angles *v.* undercut depth, as measured from the north side of the undercut (left hand side in the previous cross-sections)**

References

Albrecht, J. B., Gibson, W. H., Vakili, A., Sandy, M. P. and Ross, K. 2010. Application of advanced numerical modelling techniques for assessment of capability, subsidence and airblast hazard in a sublevel caving mine, in Proceedings of the 2nd Int. Symp. on 'Block and sublevel caving', (ed. Y. Potvin), 495–508, Perth, Australian Centre for Geomechanics.

Bullock, K., Kaiser, P. K. and Yong, S. 2012. Numerical simulations of deep block caving angles: a comparative case, in Proceedings of the 6th International Conference and Exhibition on Mass Mining, Massmin 2012, Sudbury, Ontario, Canada.

Elmo, D., Rogers, S., Beddoes, R. and Catalan, A. 2010. An integrated finite/discrete element method – discrete fracture network synthetic rock mass approach for the modelling of surface subsidence associated with panel cave mining at the Cadia East underground project, in Proc. 2nd Int. Symp. on 'Block and sublevel caving', (ed. Y. Potvin), 167–180, Perth, Australian Centre for Geomechanics.

Elmo, D. and Stead, D. 2010. An integrated numerical modelling – discrete fracture network approach applied to the characterisation of rock mass strength of naturally fractured pillars, *Rock Mech. Rock Eng.*, **43**, (1), 3–19.

Hoek, E., Carranza-Torres, C. T. and Corkum, B. 2002. Hoek–Brown failure criterion – 2002 edition, in Proceedings of the 5th North American Rock Mechanics Symposium, (eds. R. Hammah *et al.*), 267–273, Toronto, University of Toronto Press.

Hoek, E. and Diederichs, M. S. 2006. Empirical estimation of rock mass modulus, *Int. J. Rock Mech. Min. Sci.*, **43**, (2), 203–215.

Hudson, J. and Feng, X. 2010. Technical auditing of rock mechanics modelling and rock engineering design, *Int. J. Rock Mech. Min. Sci.*, **47**, (6), 877–886.

Itasca Consulting Group. 2009. FLAC3D. Version 4·0, Minneapolis, US, Itasca Consulting Group, Inc.

Itasca Consulting Group. 2010. UDEC, Version 5.0, Minneapolis, US, Itasca Consulting Group, Inc.

Munjiza, A. 2004. The combined finite-discrete element method, 348, Chichester, John Wiley & Sons.

Owen, D. R. J., Feng, Y. T., de Souza Neto, E. A., Cottrell, M. G., Wang, F., Andrade Pires, F. M. and Yu, J. 2004. The modelling of multi-fracturing solids and particulate media, *Int. J. Num. Meth. Eng.*, **60**, 317–339.

Rockfield. 2009. ELFEN, Version 4.3.3, Swansea, UK, Rockfield Software.

Rocscience. 2009. Phase2, Version 7.0, Toronto, Canada, Rocscience Inc.

Sainsbury, B. 2012. A model for cave propagation and subsidence assessment in jointed rock, PhD thesis, The University of New South Wales, Sydney.

Stead, D., Eberhardt, E. and Coggan, J. S. 2006. Developments in the characterization of complex rock slope deformation and failure using numerical techniques, *Eng. Geol.*, **83**, 217–235.

van As, A., Davison, J. and Moss, A. 2003. Subsidence definitions for block caving mines, Rio Tinto Technical Services.

Vyazmensky, A., Elmo, D. and Stead, D. 2010. Role of rock mass fabric and faulting in the development of block caving induced surface subsidence, *Rock Mech. Rock Eng.*, **43**, (5), 533–556.

Woo, K., Eberhardt, E., Elmo, D. and Stead, D. 2013. Empirical investigation and characterization of surface subsidence related to block cave mining, *Int. J. Rock Mech. Min. Sci.*, **61**, 31–42.